Overtone-induced dissociation and isomerization dynamics of the hydroxymethyl radical (CH2OH and CD2OH). II. Velocity map imaging studies

M. Ryazanov, C. Rodrigo, and H. Reisler

Citation: J. Chem. Phys. **136**, 084305 (2012); doi: 10.1063/1.3685899
View online: http://dx.doi.org/10.1063/1.3685899
View Table of Contents: http://jcp.aip.org/resource/1/JCPSA6/v136/i8
Published by the American Institute of Physics.

Overtone-induced dissociation and isomerization dynamics of the hydroxymethyl radical (CH_2OH and CD_2OH). II. Velocity map imaging studies

M. Ryazanov, C. Rodrigo, and H. Reisler[a)]
Department of Chemistry, University of Southern California, Los Angeles, California 90089-0482, USA

(Received 2 December 2011; accepted 31 January 2012; published online 24 February 2012)

The dissociation of the hydroxymethyl radical, CH_2OH, and its isotopolog, CD_2OH, following excitation in the $4\nu_1$ region (OH stretch overtone, near 13 600 cm^{-1}) was studied using sliced velocity map imaging. A new vibrational band near 13 660 cm^{-1} arising from interaction with the antisymmetric CH stretch was discovered for CH_2OH. In CD_2OH dissociation, D atom products (correlated with CHDO) were detected, providing the first experimental evidence of isomerization in the $CH_2OH \leftrightarrow CH_3O$ ($CD_2OH \leftrightarrow CHD_2O$) system. Analysis of the H (D) fragment kinetic energy distributions shows that the rovibrational state distributions in the formaldehyde cofragments are different for the OH bond fission and isomerization pathways. Isomerization is responsible for 10%–30% of dissociation events in all studied cases, and its contribution depends on the excited vibrational level of the radical. Accurate dissociation energies were determined: $D_0(CH_2OH \rightarrow CH_2O + H) = 10\,160 \pm 70$ cm^{-1}, $D_0(CD_2OH \rightarrow CD_2O + H) = 10\,135 \pm 70$ cm^{-1}, $D_0(CD_2OH \rightarrow CHDO + D) = 10\,760 \pm 60$ cm^{-1}. © *2012 American Institute of Physics*. [http://dx.doi.org/10.1063/1.3685899]

I. INTRODUCTION

The CH_2OH and its less stable isomer, CH_3O, are relevant to atmospheric and combustion chemistry, being implicated as intermediates in reactions such as $O + CH_3$ and $CH + H_2O$.[1–4] CH_2OH and CD_2OH also play an important role in the unusual deuterium enrichment of interstellar methanol.[5] The high-level electronic structure calculations reported in Part I (Ref. 6) show that the barrier heights for $CH_2OH \rightarrow CH_2O + H$ and $CH_2OH \rightarrow CH_3O$ processes are within ~400 cm^{-1} of each other and very close to the studied excitation energy range (~13 600–13 660 cm^{-1}). The barrier for $CH_3O \rightarrow H + CH_2O$ dissociation is lower than the isomerization barrier by ~1700 cm^{-1}, ensuring that CH_2OH isomerization is quickly followed by decomposition. It should be noted, however, that the rates for these two possible CH_2OH dissociation pathways depend not only on the barrier heights, but also on the character of the excited vibrational states, and thus might be highly state-specific.

Temps and co-workers studied the state-specific dissociation of the methoxy radical, using stimulated emission pumping from an excited electronic state to reach high vibrational levels of the ground electronic state, mainly in the CO stretch.[7] They determined state-specific decay rates in the tunneling regime and up to ~1500 cm^{-1} above the dissociation barrier, almost reaching the isomerization barrier top. However, no indications of isomerization to CH_2OH were observed, in agreement with the relative barrier heights. The state-specific dissociation rates showed large fluctuations and were consistent with statistical theories.

Due to experimental difficulties, there are relatively few studies of the ground electronic state of CH_2OH in spite of its importance. Most fundamental vibrations of CH_2OH and its isotopologs were observed in an Ar matrix by Jacox[8] using infrared (IR) absorption spectroscopy. Few fundamentals and several overtones and combinations of out-of-plane modes were observed in effusive molecular beam experiments by Johnson and Hudgens[9] who used resonance enhanced multiphoton ionization (REMPI) detection. In more recent studies[10] our group employed a supersonic molecular beam and IR–UV double resonance techniques to observe partially resolved rotational structure of the antisymmetric and symmetric CH stretch fundamentals (ν_2 and ν_3, respectively), as well as the OH stretch fundamental and its first overtone (ν_1, $2\nu_1$). In the following work,[11] these investigations were extended to $3\nu_1$ and $4\nu_1$ levels of CH_2OH and $4\nu_1$ of CD_2OH. The $4\nu_1$ levels of the two isotopologs lie above the dissociation thresholds and could be detected only by monitoring H photofragments, indicating a relatively fast predissociation (lifetime ~25 ps estimated from the spectral linewidths) of the hydroxymethyl radical at this energy. That work was the only known experimental study of the predissociation dynamics of the hydroxymethyl radical.

The observation of predissociation induced by OH stretch overtone excitation is intriguing because the OH stretch is the reaction coordinate leading to $CH_2O + H$, as opposed to other cases of overtone-induced dissociation,[12] where the excited bond was not broken in the dissociation and retained its bound character even above the dissociation threshold. The existence of a barrier for CH_2OH dissociation was assumed to be the reason why the OH stretch preserved its character of a bound vibration. Despite the fact that the available calculations,[3,13] all placed the barrier for isomerization to methoxy lower than the barrier for OH bond fission, no D products from CD_2OH were detected. Therefore, it was concluded that isomerization to CHD_2O was at best a minor channel, and that the

a)Author to whom correspondence should be addressed. Electronic mail: reisler@usc.edu.

dissociation proceeded by tunneling through the barrier to $CH_2O + H$.

In our previous studies, we could not investigate the dynamics of the hydroxymethyl radical predissociation because the time-of-flight (TOF) detection method that we employed did not have sufficient resolution to reveal structure in the H fragment kinetic energy distribution (KED). We have therefore replaced it with a sliced velocity map imaging (SVMI) arrangement which allowed us to obtain internal energy distributions of CH_2O, CHDO, and CD_2O cofragments from images of H^+ and D^+ following dissociation of CH_2OH and CD_2OH.

The major experimental complication in our studies involved contributions from dissociation upon electronic excitation to the 3*s* and 3*p* Rydberg states[14] by 2- and 3-photon absorption at the high laser intensities needed to effect excitation of the $4\nu_1 \leftarrow 0$ transition. While this multiphoton excitation gives rise predominantly to H fragments with high velocities, in the usual velocity map imaging (VMI) setup the projections of these high velocities on the two-dimensional detector contribute to signal at both large and small radii of the raw image. In image reconstruction, these large interfering signals lead to unacceptable background noise in the region of the image that contains contributions from one-photon dissociation. For situations like this, the SVMI method[15] is advantageous because there is no need for image reconstruction. It is therefore possible to record only the one-photon region of the image, effectively discriminating against background signals at high kinetic energies, and to obtain photofragment yield spectra with resolved translational energies, i.e., correlated with specific vibrational levels of the formaldehyde cofragment.

This article presents our results on the overtone-induced dissociation dynamics of CH_2OH and CD_2OH, with special emphasis on the role of isomerization to CH_3O (CHD_2O). Observation of a D product from CD_2OH provides direct evidence of isomerization in the $CD_2OH \leftrightarrow CHD_2O$ system. Analysis of the formaldehyde products rovibrational state distributions shows that they are qualitatively different for the two decomposition channels (OH bond fission and isomerization followed by dissociation), and this allows us to estimate the state-specific branchings between these two pathways.

II. EXPERIMENTAL ARRANGEMENT AND PROCEDURES

The experimental procedures for the preparation of CH_2OH samples and detection of H and D atoms were similar to those used in our previous studies[10,11] and are described only briefly here. A molecular beam of CH_2OH (CD_2OH) radicals was created in the source chamber, skimmed, and introduced into the differentially pumped detection chamber, where the radicals were dissociated by focused visible laser radiation. H (D) products were ionized by a counterpropagating laser radiation using REMPI, and the H^+ (D^+) ions were detected by SVMI. Two kinds of measurements were performed: (1) the dependence of fragment yields on excitation wavelength (action spectra); (2) velocity distributions of the fragments.

CH_2OH (CD_2OH) radicals were produced as before by the reaction of CH_3OH (CD_3OH) with Cl atoms. Typically a mixture of 3% methanol[32] and 1% Cl_2 (by volume) in ~1.5 bar of helium was introduced into a piezoelectrically driven pulsed nozzle that has a quartz tube attached to it. Cl_2 molecules were dissociated inside the quartz tube by 355 nm laser light (3rd harmonic of Quanta-Ray GCR11 Nd:YAG laser, ~20 mJ, focused with 15 cm focal length (f.l.) cylindrical lens). The molecular beam with reaction products was introduced into the detection chamber through a skimmer (Beam Dynamics, ø1 mm). The rotational temperature of the radicals in the detection region was 10–15 K.

The radical excitation radiation was generated by a Nd:YAG laser pumped dye laser (Continuum PL8000/ND6000, LDS 722 dye, ~35 mJ; 0.1 cm^{-1}, 30 cm f. l. lens). H (D) fragments were ionized using a $1 + 1'$ REMPI scheme through the $2p \leftarrow 1s$ transition. The radiation near Lyman-α (82 290 cm^{-1}, 121.6 nm) was generated, as described before,[11] by frequency tripling 2–3 mJ of the doubled output of a Nd:YAG pumped dye laser (Continuum NY-81C/ND6000, LDS 751 dye, Inrad Autotracker-II doubler with KDP-D crystal) in a Kr/Ar gas cell.[16] The unconverted part of the radiation passing through the tripling cell was used for near-threshold ionization of the excited H (D) atoms. Because the bandwidth of the detection laser was narrower than the Doppler profile of the H (D) fragments, velocity map images were recorded by frequency scanning of the laser across the Doppler profile to achieve unbiased detection efficiency. However, for recording action spectra such scans take too long, and since qualitative KEDs are sufficient, the detection frequency was fixed at a value optimized for best one-photon signal.

The main modification in the experimental arrangement was the incorporation of inline SVMI for detection of H^+ (D^+) ions. The SVMI method has been described before, and the difficulties in implementing it for light H and D ions were explained.[15] A full description of our experimental arrangement will be given elsewhere; here we describe briefly the essential components and performance characteristics.

In general terms, the ion optics consists of an immersion electrostatic lens resembling the arrangement described in Ref. 15 for acceleration and focusing of ions, and an einzel lens installed in the drift region for additional control of the image magnification (see Ref. 17 for a similar approach). With this system the TOF focusing[18] and velocity map focusing[19] conditions can be satisfied simultaneously, and the temporal stretching of the ion cloud required for slicing is independent of the imaged kinetic energy range.

To achieve thin time slices, we have built a fast high-voltage pulser based on the design given in Ref. 20. The effective slice profile, determined by convolution of the ionization laser pulse time profile, the MCP gain variation controlled by the electric pulse shape, and the relative timing jitter distribution, is nearly Gaussian with FWHM of ~5 ns. The VMI conditions are chosen such that the total time spread of the ion cloud is ~50 ns, leading to reasonable collection efficiency with sufficient resolution ($\Delta E/E \approx 1\%$).

Imaging data from the detector (Galileo/Photonis, ø40 mm microchannel plate chevron stack) are recorded at

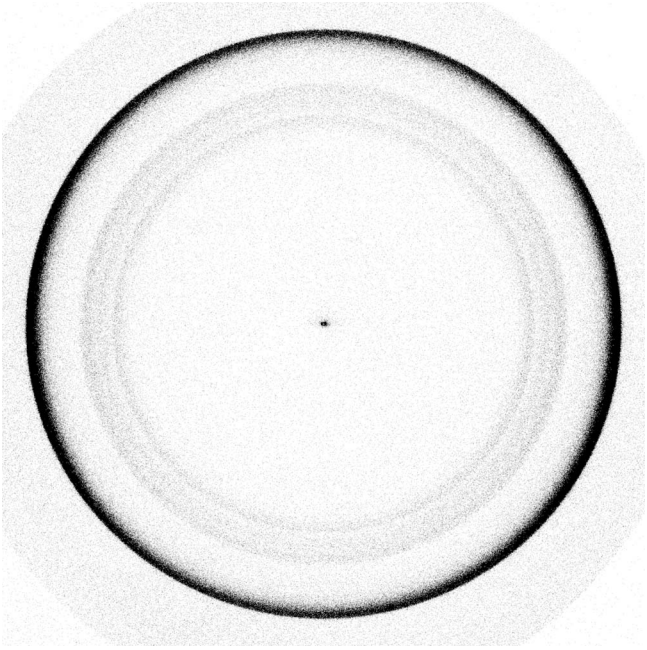

FIG. 1. Sliced velocity map image obtained by monitoring H fragments from CH_2OH dissociation at 13 602 cm^{-1}. The intense outer ring correlates with vibrationless CH_2O cofragment. The weak inner rings correspond to CH_2 rock, wag, and scissors, and CO stretch excitations in the CH_2O.

1 megapixel resolution (PixeLink PL-B741F CMOS camera, Tamron 23FM25SP *f*/1.4 lens). The positions of ion spots for each laser pulse are analyzed by a centroiding algorithm similar to the one described before,[21] and the coordinates with a time stamp are saved to a file for further analysis. An example of a typical image obtained by monitoring H photofragments from CH_2OH is shown in Fig. 1.

Kinetic energy release (KER) distributions are obtained by binning all recorded ion positions into small speed intervals and converting the H (D) speed distribution to KED in the usual way. Kinetic energy calibration was performed by using the photodissociation of O_2, HBr, and H_2S. It showed excellent agreement with the predictions obtained with the ion optics simulation software package SIMION 8 (Ref. 22) ($\sim$1% difference in kinetic energy) in all modes of operation, and therefore numerical simulations were used for selection of the optimal ion optics parameters and analysis of the recorded images.

Action spectra are obtained by changing the excitation laser frequency in small steps while continuously running SVMI detection. Time stamps for each frequency are recorded, allowing subsequent binning of the detected ion distributions by laser frequency intervals. The results are analyzed as (1) two-dimensional spectra, i.e., ion yield as a function of the excitation frequency and ion speed and (2) state-resolved photofragment yield spectra, by integration of the two-dimensional spectrum over selected speed intervals.

The application of SVMI in our experiment significantly enhanced the detection sensitivity because of the following:

1. The use of event counting essentially eliminates detection background noise; only statistical fluctuations of the signal remain. This allowed us to observe small signals and to improve the signal-to-noise ratio (SNR) by increasing the accumulation time, limited only by stability of the experimental conditions.
2. Velocity resolution allows discrimination between signals from the studied one-photon process and those generated by spurious processes, such as photodissociation of the radical by the detection laser and/or multiphoton absorption of the excitation radiation. This is important in our case because both of these processes are sometimes more efficient than the overtone-induced dissociation. Although some interfering signals (e.g., from photodissociation of unreacted methanol in the molecular beam) remain, most of this background has higher kinetic energy and is easily rejected.
3. The measured KEDs allow unambiguous identification of the dissociation cofragment through its vibrational structure, and the parent radical by the observed kinetic energy maximum (which should be consistent with the corresponding dissociation energy). This has permitted us to increase the radical production yield without the risk of possible signal contamination by reaction byproducts.

III. EXPERIMENTAL RESULTS AND ANALYSIS

A. Action spectra

Figure 2 shows action spectra for photodissociation of CH_2OH and CD_2OH obtained by monitoring H (D) photofragments in the region of the previously observed $4\nu_1 \leftarrow 0$ transition.[11] Each spectrum is derived from data obtained as described in Sec. II. In monitoring H fragments, only the signal correlated with one-photon excitation and the formaldehyde cofragment in the ground vibrational state (which is the most populated, see below) is plotted. Signals correlated with vibrationally excited cofragments were significantly smaller but had identical excitation wavenumber dependencies. Background in the images was relatively small at kinetic energies corresponding to one-photon signals and thus is not subtracted in the plots.

The bands near 13 600 cm^{-1} for CH_2OH and 13 620 cm^{-1} for CD_2OH (Figs. 2(a) and 2(b), respectively) are in good agreement with previous results,[11] but have much better SNR. With CH_2OH excitation, an additional band near 13 660 cm^{-1} was observed in the present work. It has narrower linewidths and 4–5 times lower integrated intensity than the main band. In contrast, CD_2OH did not show other detectable bands within $\pm$100 cm^{-1} of the observed band. As discussed below, the two bands in CH_2OH arise from an accidental resonance with another state involving the antisymmetric CH stretch.

The higher SNR achieved in the present work enabled us to detect also a small amount of D products from CD_2OH dissociation. Figure 2(c) shows the D fragment yield spectrum from CD_2OH, which is correlated with CHDO cofragments. As with the other bands, all state-resolved action spectra had identical shapes. However, in contrast to the H fragment channel, the fraction of vibrationally excited cofragments was significant. Therefore, the signal correlated with all vibrational

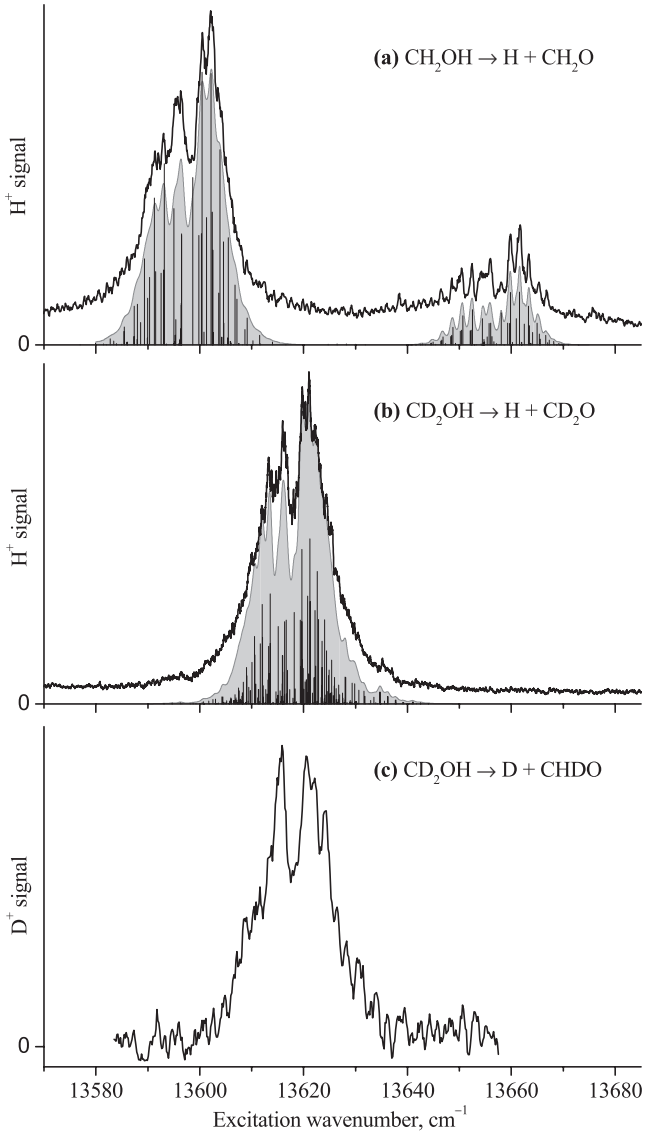

FIG. 2. Action spectra for CH_2OH and CD_2OH one-photon dissociation obtained by monitoring H (D) products. Reactions are indicated in the figure. Solid curves show experimental data. Rovibrational band fits are represented by shaded areas (contours) and lines (spectral line positions and intensities), vertically displaced for clarity. See text for details.

states of CHDO was collected in order to improve the SNR. When monitoring the small D photofragment signal, it was necessary to subtract background contributions. They were estimated by interpolation between the background signal obtained at lower and higher kinetic energies than those produced by one-photon predissociation of CD_2OH and smoothing over excitation wavenumbers. The background comes mostly from multiphoton dissociation by the excitation laser.

It is evident from comparison of Figs. 2(b) and 2(c) that the D and H fragments come from the same source, namely, CD_2OH overtone-induced dissociation. The small deviations in the shapes of the bands are probably due to the high noise level in the D spectrum and not to rotational state specificity in the processes producing H and D.

The action spectra were analyzed using PGOPHER, a program for simulating rotational structure.[23] Each band was fitted separately to a single vibrational transition under the rigid asymmetric rotor approximation and assuming thermal rotational distribution of the radicals. The rotational constants for the ground vibrational state were fixed at the most recent theoretical values[6] (they are in reasonable agreement with previously reported calculations[24]). The band origin, the excited vibrational state rotational constants, the Lorentzian linewidth and the rotational temperature were found by nonlinear least-square fitting (NLSF) of the partially resolved rotational structure. Excitation laser bandwidth was accounted for by Gaussian broadening with FWHM of 0.1 cm^{-1}. Since the CD_2OH spectrum lacks a pronounced structure, the fit was relatively insensitive to variations of rotational constants, and they were fixed at the theoretical values. The NLSF procedure also failed to converge for the linewidth, thus its confidence interval was determined by visual inspection. Additional details are given in the supplementary material.[25]

The results of the fittings are presented in Fig. 2 (see also supplementary material for more detailed plots). Only *a*-type transitions were used in the fits for CH_2OH, as addition of *b*-type transitions did not improve the goodness of the fits. The large band of CH_2OH was best fit with a band origin $\nu_0 = 13\,596.9 \pm 1$ cm^{-1} (the uncertainty includes laser calibration error), a linewidth of 1.6 ± 0.3 cm^{-1} and rotational constants $A' = 6.10(3)$ cm^{-1}, $B' = 0.964(4)$ cm^{-1}, $C' = 0.841(5)$ cm^{-1} (standard deviations of the fit in units of the least significant digit are given in parentheses), in reasonable agreement with the previous results.[11] The small band was fit with a band origin $\nu_0 = 13\,656.2 \pm 1$ cm^{-1}, a linewidth of 0.7 ± 0.1 cm^{-1} and similar rotational constants $A' = 6.09(2)$ cm^{-1}, $B' = 0.995(3)$ cm^{-1}, $C' = 0.822(4)$ cm^{-1}. Rotational constants for both upper states agree well with the *ab initio* values.[6] The CD_2OH spectrum was more difficult to fit, and the best least-square fit was obtained with about 25% (by intensity) of *b*-type transition included, $\nu_0 = 13\,616.7 \pm 1$ cm^{-1} and a linewidth of 1.2 ± 0.2 cm^{-1}. Neither of the fits satisfactorily described the overall shapes of the observed bands. A possible reason for this is discussed in Sec. IV A.

B. Kinetic energy release distributions

KEDs correlated with one-photon dissociation were obtained for H and D fragments as described in Sec. II. No noticeable variations in the KEDs within the frequency span of each spectral band were observed. Therefore, quantitative measurements were performed only at excitation frequencies of maximum signal in each band: 13 602 cm^{-1} and 13 662 cm^{-1} for CH_2OH and 13 621 cm^{-1} for CD_2OH (H and D channels). The results are presented in Fig. 3. In all experiments the background was unstructured in the relevant kinetic energy ranges; its intensity was relatively small for the H signals and comparable in size to the D signal. The background is subtracted in all shown plots.

The velocity distributions for overtone-induced dissociation were isotropic within experimental accuracy.[33] Rotational structure in the formaldehyde cofragment was not resolved. Vibrational structure was resolved, but due to significant rotational excitation in the product the rotational

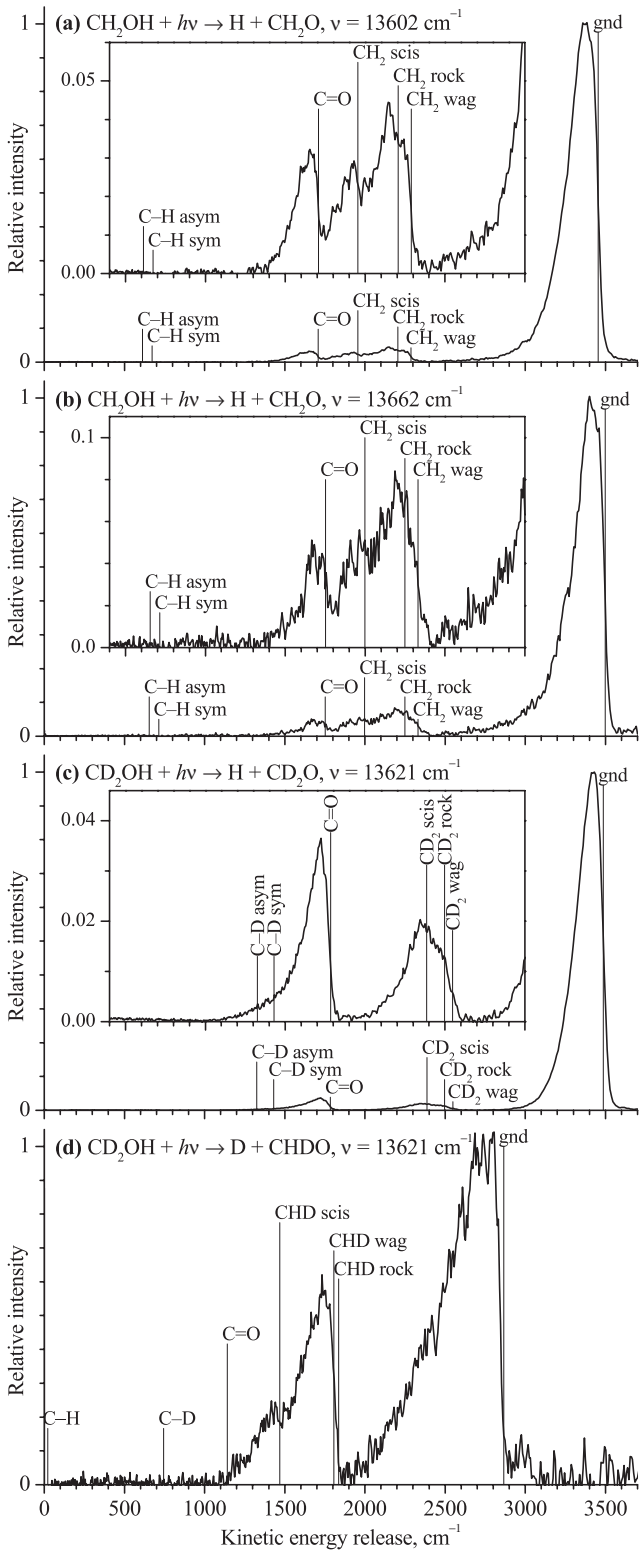

FIG. 3. Kinetic energy release distributions in CH_2OH and CD_2OH one-photon dissociation obtained by monitoring H (D) products. Reactions and excitation energies are indicated in the figure. Origins of vibrational levels of the formaldehyde cofragment (see Table II) are marked by vertical lines. Insets show the lower KER parts with expanded vertical scale.

envelopes of most of the vibrational states were partially overlapped.

Each of the KEDs was analyzed separately by fitting the rovibrational contour with PGOPHER.[23] The rotational constants and energies of vibrational levels of formaldehyde isotopologs used in the fitting were compiled from experimental data available in the literature (see Table II). The dissociation energy (D_0), the experimental broadening (modeled with a Gaussian function) and the ground state rotational temperature were determined by least squares fitting of the KED part corresponding to vibrationless formaldehyde. Then the remaining part of the KED was fitted to determine the rotational temperature of vibrationally excited levels and their relative populations. The results are summarized in Tables I and II. The fits and their comparison to the experimental KEDs are shown in the supplementary material.[25]

TABLE I. Dissociation energies (D_0) determined from kinetic energy distributions of H and D fragments. The confidence intervals include energy calibration and KED fitting uncertainties.

Reaction	D_0 (cm^{-1})
$CH_2OH \rightarrow H + CH_2O$	$10\,160 \pm 70$
$CD_2OH \rightarrow H + CD_2O$	$10\,135 \pm 70$
$CD_2OH \rightarrow D + CHDO$	$10\,760 \pm 60$

The dissociation energies for all three observed reactions are consistent with estimated isotopic zero-point energy differences. The latest theoretical predictions[6,24] of the dissociation energies lie within the confidence intervals of our results.

The rotational profiles are fit fairly well by thermal distributions. However, since there is no reason to expect local thermodynamic equilibrium among the rotational levels within each vibrational state, these *effective* temperatures should be considered only as a measure of the extent of rotational excitation. Significant overlaps of the contours for vibrationally excited levels did not allow meaningful determination of their individual temperatures, thus a common temperature, different from that of the ground state, was used. The overlaps also caused large correlations among the derived populations, especially for rock and wag excitations which are close in energy. Because of these problems we ascertained that the total fraction of excited state populations obtained from the fits and by direct integration of the excited states part of the KED are in good agreement (see Table II). The quoted uncertainties do not include systematic errors due to nonuniform detection efficiency, which can be assessed at a few percent. These errors, however, are consistent for all KEDs and thus should not affect the analysis discussed below (Sec. IV B).

IV. DISCUSSION

The most intriguing result of the present study is the observation of H and D products from CD_2OH having very different KEDs (Fig. 3). The detection of D products from overtone-induced dissociation of CD_2OH indicates that in addition to dissociation by OH bond fission, isomerization to methoxy also takes place. As shown in previous work,[29] the CH bond strength in CH_2OD is ~27 400 cm^{-1}, much greater than both the OH bond strength in CD_2OH (~10 100 cm^{-1}) and the one-photon excitation energy (<14 000 cm^{-1}); thus CD bond fission in CD_2OH is impossible. Yet, the barrier height for isomerization to CHD_2O is only ~13 800 cm^{-1},

TABLE II. Formaldehyde fragment rovibrational distribution parameters obtained from fitting of H and D cofragment kinetic energy distributions (standard deviations in units of the least significant digit are given in parentheses).

				Relative population (fit)[b]			
	Energy[a] (cm^{-1})			$CH_2OH \rightarrow H + CH_2O$		CD_2OH (13 621 cm^{-1})	
Fragment excitation	CH_2O	CD_2O	CHDO	13 602 cm^{-1}	13 662 cm^{-1}	$H + CD_2O$	$D + CHDO$
Ground	0	0	0	1	1	1	1
C=O	1746	1702	1724	0.0219(5)	0.0294(10)	0.0333(2)	0
Scissors	1500	1100	1396	0.0179(5)	0.0300(11)	0.0103(3)	0.062(3)
Rock	1249	989	1028	0.0212(7)	0.0466(17)	0.0083(6)	0.151(9)
Wag	1167	938	1059	0.0211(7)	0.0377(17)	0.0091(5)	0.185(9)
Excited fraction (%)		Fit		7.6	12.6	5.7	28.8
		Integration		7.8	12.8	5.9	28.4
T_{rot}^{eff} (K)		Ground		145(10)	155(10)	120(5)	320(20)
		Excited		110(10)	140(20)	130(15)	180(15)

[a]Experimental vibrational energies taken from Refs. 26 (CH_2O), 27 (CD_2O), and 28 (CHDO).
[b]Population estimations for rock and wag are strongly correlated ($\rho \sim -0.8$) in all cases due to a significant overlap of their rotational envelopes.

and the barrier for $CHD_2O \rightarrow D + CHDO$ dissociation is even lower ($\sim$12 600 cm^{-1}).[6] We conclude therefore that D atoms are produced by isomerization followed by dissociation.

A. Overtone spectroscopy and state interactions

The action spectra and their analyses are in agreement with previous results,[11] except that with better SNR we are able to observe an additional band near 13 660 cm^{-1}. Based on previous analysis, it appears that the zeroth-order $4\nu_1$ state carries most of the oscillator strength for the observed transitions. However, in this work we demonstrate that it is mixed in CH_2OH with another close-lying vibrational state. The mixing does not occur in CD_2OH, reinforcing the interpretation that the interaction derives from an accidental near-resonance specific to CH_2OH. A very similar situation exists in the overtone spectroscopy of CH_3OH, where $5\nu_1$ is strongly mixed with $4\nu_1 + \nu_2$ (ν_1 is the OH stretch and ν_2 is one of the asymmetric CH stretches), and this interaction is also affected by isotopic substitutions.[30]

In CH_2OH the lower-frequency level of the coupled pair lies very close to the $4\nu_1$ energy extrapolated from the lower ν_1 overtones,[11] whereas the higher-frequency level is close to the sum of the $3\nu_1$ and ν_2 levels (10 484 + 3162 = 13 646 cm^{-1}, using the values from Refs. 11 and 10). Since the ν_2 mode has weaker IR intensity than ν_1,[10,24] the 4–5 times lower relative integrated intensity of the higher-frequency band is consistent with this assignment (although the zeroth-order $3\nu_1 + \nu_2$ state could be excited directly, its dissociation without coupling to $4\nu_1$ is unlikely, as discussed below). The vibrational configuration interaction (VCI) calculations reported in Part I (Ref. 6) support this analysis, showing that both bright states found in this region have large contributions from $4\nu_1$ and $3\nu_1 + \nu_2$ basis functions.

Based on the similarity in the linewidths of the transitions to $4\nu_1$ in CH_2OH and CD_2OH, it was suggested previously that the linewidths are dominated by the dissociation rate.[11] Otherwise, one might expect substantially different broadenings for the two isotopologs, which have different densities of states and couplings. We confirm that the bands that are mostly $4\nu_1$ have similar linewidths, but the band with a large $3\nu_1 + \nu_2$ contribution has noticeable narrower lines (see Sec. III A). This suggests state-specificity in the dissociation, as discussed below.

Our inability to fit well the action spectra with isolated transitions is quite likely caused by the presence of other weakly absorbing states arising from weaker couplings of the bright states discussed above with combinations of lower frequency vibrations. The inclusion of a *b*-type transition to improve the fit shown in Fig. 2(b) might therefore be misleading and simply serve as apparent compensation of small contributions from other bands.

B. Product state distributions

The analysis of the H and D KEDs summarized in Table II sheds light on the dissociation dynamics of the hydroxymethyl radical in the ground electronic state. The dissociation of the CD_2OH isotopolog enables us to distinguish between the H atom initially in the OH group (which carries most of the optical excitation) and the D atoms initially attached to the carbon atom, and thus observe the isomerization channel explicitly. Such distinction, however, is impossible for CH_2OH. Nevertheless, analysis of the experimental results indicates that isomerization is responsible for a fraction of H products in both radical isotopologs.

We note that when monitoring D from CD_2OH, there is no CO stretch excitation in the formaldehyde cofragment, whereas all H-producing reactions lead to a small but quite consistent population ($\sim$3%) in this mode. In contrast, methylene group deformation modes (scissors, rock, and wag) are significantly excited ($\sim$28% total population) in the D-producing reaction, but show smaller and variable excitations when monitoring H. These observations suggest that direct OH bond fission produces formaldehyde that is predominantly vibrationless or has small CO stretch excitation, but excitation of the deformation modes is associated mainly with the isomerization channel contribution that is different in each case. The positive correlation between the effective rotational temperatures and the extent of the deformation modes

TABLE III. Formaldehyde vibrational populations predicted by the model described in Sec. IV B. Deviations from the experimental values in units of the least significant digit are given in parentheses.

	Relative population				
	$CH_2OH \rightarrow H + CH_2O$		CD_2OH (13 621 cm^{-1})		
Fragment excitation	13 602 cm^{-1}	13 662 cm^{-1}	$H + CD_2O$	$D + CHDO$	Direct dissociation[a]
Ground	1	1	1	1	1
C=O	0.0293(+74)	0.0251(−43)	0.0320(−13)	0.000(+00)	0.0320–0.0333
Scissors	0.0160(−20)	0.0234(−65)	0.0113(+10)	0.068(+12)	0.0113–0.0089
Rock	0.0218(+06)	0.0450(−16)	0.0072(−11)	0.183(+07)	0.0072–0.0000
Wag	0.0218(+07)	0.0414(+37)	0.0095(+04)	0.158(−12)	0.0095–0.0034
% Isomerization	11–15	26–30	0–5	100	0

[a]Isomerization channel distribution can be seen in the D + CHDO column.

excitations indicates that rotational excitation is lower for direct OH bond fission and higher for dissociation after isomerization.[34]

In order to estimate the branching between isomerization and direct dissociation, the experimental vibrational population distributions were analyzed in terms of a simple model with the following assumptions:

1. The products observed in each experiment come from two independent dissociation channels (direct and through isomerization), and thus the observed distributions are linear combinations of the distributions for each channel.
2. The distribution for each of the two channels is the same in all experiments. That is, it does not depend on isotopic substitution effects and variations in the radical excitation energy in the narrow range (∼100 cm^{-1}) used in the present experiments.

These assumptions allow us to write 16 equations (four vibrational populations in four experiments) for the observed relative populations $p_{e,v}$ of state v in experiment e:

$$p_{e,v} = (1 - k_e)p_{\mathrm{d},v} + k_e p_{\mathrm{i},v}, \tag{1}$$

where $p_{\mathrm{d},v}$ and $p_{\mathrm{i},v}$ are the populations of state v for the direct and isomerization channels, respectively, and k_e is the fractional contribution of isomerization channel in experiment e. Normalization to $p_{e,0} = 1$ is automatically satisfied by setting $p_{\mathrm{d},0} = p_{\mathrm{i},0} = 1$. For the $CD_2OH \rightarrow D + CHDO$ experiment the value $k_e = 1$ is known, and thus the 16 equations have 11 unknowns: 4 excited vibrational populations for each of the 2 channels plus the isomerization contributions k_e in 3 experiments.

The system of nonlinear equations was solved numerically by minimization of weighted squared error (using covariance matrices for the experimental populations obtained in the KED fittings) under the constraints $p_{\mathrm{d},v} \geq 0$, $p_{\mathrm{i},v} \geq 0$, and $0 \leq k_e \leq 1$. Despite the fact that the number of unknowns is smaller than the number of equations, the system has one degree of freedom. Namely, (1) can be recast as

$$p_{e,v} = (1 - k_e)p_{\mathrm{d},v} + k_e p_{\mathrm{i},v} = (1 - k'_e)p'_{\mathrm{d},v} + k'_e p_{\mathrm{i},v}, \tag{2}$$

$$\begin{cases} p'_{\mathrm{d},v} = (1 + \alpha)p_{\mathrm{d},v} - \alpha p_{\mathrm{i},v} \\ k'_e = (k_e + \alpha)/(1 + \alpha), \end{cases} \tag{3}$$

for any α. This variation, however, is limited by $p_{\mathrm{d},v} \geq 0$, $k_e \geq 0$ restrictions, which are reached at $p_{\mathrm{d},v} = 0$ for rock population on one side and $k_e = 0$ for $CD_2OH \rightarrow H + CD_2O$ experiment on the other. The model results are summarized in Table III, where the percentage of products from isomerization refers to the total yield and was calculated as $k_e \sum_v p_{i,v} / \sum_v p_{e,v}$. Detailed plots comparing the experimental KEDs and those obtained by using the model are shown in the supplementary material.[25] It is evident that the uncertainty caused by underdeterminacy of the system is relatively small and does not affect the usability of the results.[35]

As can be seen from comparing Tables II and III, this simple model reproduces the experimental results fairly well, except the CO population for the main band of CH_2OH, for which the discrepancy is ∼16 standard deviations of the fit and ∼1/3 of the observed value. This disagreement is most probably a result of deviations from the second assumption of the model and does not undermine the qualitative conclusions. The model outcome is that in CH_2OH dissociation 11%–15% of the events proceed by isomerization when the excited level is dominated by $4\nu_1$, whereas the corresponding branching for the level dominated by $3\nu_1 + \nu_2$ is larger, 26%–30%. In dissociation of CD_2OH from a purer $4\nu_1$ level, isomerization accounts for <13% events (estimated from <5% fraction for the H channel).

It is noteworthy that no excitation of CH (CD) stretch vibrations in the formaldehyde products was observed in either reaction, even though the VCI calculations[6] show that the involved CH_2OH (CD_2OH) excited states contain considerable antisymmetric CH (CD) stretch contributions, and the CD frequencies in CD_2O and CHDO are rather similar to the CO frequencies.

C. Competition between OH bond fission and isomerization

The radical decomposition mechanism in the experiments reported above is not immediately obvious. On the one hand, one might expect that excitation of vibrations with principally OH stretch character and energies very close to the barrier height for OH bond fission should lead to relatively

quick dissociation. However, while this fission is actually observed, its rate is too low (the barrier height estimated from the dissociation rate[11] is ~1000 cm^{-1} higher than the present *ab initio* value). On the other hand, the isomerization barrier is lower by ~400 cm^{-1} than the barrier for OH bond fission. Nevertheless, the isomerization rate is even smaller than the OH bond fission rate (but is not negligible).

The calculations[6] in fact show that the lowest barrier for OH bond fission corresponds to the geometry with the OH group twisted from the quasiplanar structure of the radical[6,24] such that the HOC plane becomes perpendicular to the HCH plane. The isomerization pathway involves the same OH group torsion, but additionally requires a large change of the HOC angle (see Fig. 2 in Ref. 6). Therefore, the OH stretch overtone excitation is not an effective way to promote dissociation and is even less effective for isomerization, leading to relatively long lifetimes of the vibrationally excited states.

Assuming that the observed spectral linewidths are determined by upper state lifetimes dominated by dissociation rates, it appears that the overall dissociation rate from the level that is of purer $4\nu_1$ composition is nearly twice higher than the rate from the level with smaller $4\nu_1$ contribution. At the same time the observed *fraction* of isomerization products shows the opposite trend (approximately twice the total hydrogen yield from isomerization for the longer-lived state). These observations suggest that the isomerization rate is largely insensitive to the initial state composition, whereas the OH bond fission rate decreases when the state has a smaller $4\nu_1$ component. Indeed, the state dominated by $3\nu_1 + \nu_2$ must have smaller wavefunction amplitudes at large OH distances than the state dominated by $4\nu_1$, which explains its lower dissociation rate (regardless of whether tunneling or passing just above the barrier is involved), even though the total excitation energy is slightly higher. Since the isomerization transition state has less extended OH distance,[6] the isomerization rate should be less sensitive to the degree of OH stretch excitation.

A quantitative description of these decomposition processes would require quantum-mechanical calculations in at least three dimensions (OH stretch, torsion, and HOC bending), and perhaps full dimensionality to adequately describe the product state distributions (although CH (CD) stretches are not excited in the products, they must participate in the $CD_2OH \rightarrow CHD_2O \rightarrow D + CHDO$ process).

V. CONCLUSIONS

The overtone-induced dissociation of CH_2OH and CD_2OH was studied experimentally at energies near the barrier tops for OH bond fission and isomerization to methoxy. Hydrogen products were monitored by SVMI, and action spectra and KEDs were measured in the region of excitation to $4\nu_1$. The action spectrum of CD_2OH showed only a transition to the $4\nu_1$ overtone, whereas two bands were observed in CH_2OH in the corresponding excitation region. These bands were assigned as transitions to two coupled states, the more intense band dominated by $4\nu_1$ and the less intense one by $3\nu_1 + \nu_2$.

KEDs obtained from SVMI data show distinct dynamical signatures in the formaldehyde cofragment associated with OH bond fission and isomerization to methoxy. Dissociation proceeding by OH bond fission leads mainly to formaldehyde in the vibrationless state, with a small (~3%) excitation in the CO stretch and yet smaller excitations in the methylene deformation modes (scissors, rock, and wag). On the other hand, dissociation following isomerization leads to formaldehyde that is rotationally hotter and has a much larger fraction (~28%) of the energy deposited in methylene deformations, but not in the CO stretch. No excitation in the CH (CD) stretches was observed in formaldehyde from either reaction. Analysis of the data also suggests that the dissociation rate for OH fission depends more strongly on the initially excited level than the isomerization rate, at least for the levels examined in this study.

The $CH_2OH \leftrightarrow CH_3O$ dissociative system has proven to be amenable to detailed experiments on its dynamics in the ground electronic state. Most of the previous experimental work[7,31] has dealt with initial excitation of CH_3O for which isomerization is unlikely by energetic considerations. Our work is the first detailed study of excitation and dissociation of CH_2OH and CD_2OH that demonstrates the role of isomerization. We hope in the future to extend the experimental studies to higher energies, other vibrational overtones and combination bands and rotationally resolved states by employing IR-IR double resonance excitation techniques.

ACKNOWLEDGMENTS

Support by the (U.S.) Department of Energy (DOE) (Grant No. DE-FG02-05ER15629) is gratefully acknowledged. The authors thank Eugene Kamarchik, Joel Bowman, and Anna Krylov for sharing their theoretical results.

[1] P. W. Seakins and S. R. Leone, J. Phys. Chem. **96**, 4478 (1992); W. Hack, M. Hold, K. Hoyermann, J. Wehmeyer, and T. Zeuch, Phys. Chem. Chem. Phys. **7**, 1977 (2005).
[2] J. Lindner, R. A. Loomis, J. J. Klaassen, and S. R. Leone, J. Chem. Phys. **108**, 1944 (1998); C. Fockenberg, G. E. Hall, J. Preses, T. J. Sears, and J. T. Muckerman, J. Phys. Chem. A **103**, 5722 (1999); V. D. Knyazev, J. Phys. Chem. A **106**, 8741 (2002); N. Balucani, F. Leonori, A. Bergeat, R. Petrucci, and P. Casavecchia, Phys. Chem. Chem. Phys. **13**, 8322 (2011).
[3] T. P. Marcy, R. R. Díaz, D. Heard, S. R. Leone, L. B. Harding, and S. J. Klippenstein, J. Phys. Chem. A **105**, 8361 (2001).
[4] A. Bergeat, S. Moisan, R. Méreau, and J.-C. Loison, Chem. Phys. Lett. **480**, 21 (2009).
[5] T. P. M. Goumans and J. Kästner, J. Phys. Chem. A, **115**, 10767 (2011).
[6] E. Kamarchik, C. Rodrigo, J. M. Bowman, A. I. Krylov, and H. Reisler, J. Chem. Phys. **136**, 084304 (2012).
[7] A. Geers, J. Kappert, F. Temps, and J. W. Wiebrecht, J. Chem. Phys. **99**, 2271 (1993); S. Dertinger, A. Geers, J. Kappert, J. W. Wiebrecht, and F. Temps, Faraday Discuss. **102**, 31 (1995).
[8] M. E. Jacox, Chem. Phys. **59**, 213 (1981).
[9] R. D. Johnson III and J. W. Hudgens, J. Phys. Chem. **100**, 19874 (1996).
[10] L. Feng, J. Wei, and H. Reisler, J. Phys. Chem. A **108**, 7903 (2004).
[11] J. Wei, B. Karpichev, and H. Reisler, J. Chem. Phys. **125**, 034303 (2006).
[12] D. W. Chandler, W. E. Farneth, and R. N. Zare, J. Chem. Phys. **77**, 4447 (1982); M.-C. Chuang, J. E. Baggott, D. W. Chandler, W. E. Farneth, and R. N. Zare, Faraday Discuss. Chem. Soc. **75**, 301 (1983); X. Luo, P. R. Fleming, T. A. Seckel, and T. R. Rizzo, J. Chem. Phys. **93**, 9194 (1990); D. Luckhaus, J. L. Scott, and F. F. Crim, J. Chem. Phys. **110**, 1533 (1999); B. Kuhn and T. R. Rizzo, J. Chem. Phys. **112**, 7461 (2000); F. Reiche, B. Abel, R. D. Beck, and T. R. Rizzo, J. Chem. Phys. **112**, 8885 (2000).

[13]S. Saebø, L. Radom, and H. F. Schaefer III, J. Chem. Phys. **78**, 845 (1983).
[14]V. Aristov, D. Conroy, and H. Reisler, Chem. Phys. Lett. **318**, 393 (2000); D. Conroy, V. Aristov, L. Feng, and H. Reisler, J. Phys. Chem. A **104**, 10288 (2000); L. Feng, X. Huang, and H. Reisler, J. Chem. Phys. **117**, 4820 (2002); L. Feng, A. V. Demyanenko, and H. Reisler, J. Chem. Phys. **118**, 9623 (2003); L. Feng and H. Reisler, J. Phys. Chem. A **108**, 9847 (2004).
[15]J. J. Lin, J. Zhou, W. Shiu, and K. Liu, Rev. Sci. Instrum. **74**, 2495 (2003).
[16]R. Mahon, T. J. McIlrath, V. P. Myerscough, and D. W. Koopman, IEEE J. Quantum Electron. **15**, 444 (1979).
[17]G. A. Garcia, L. Nahon, C. J. Harding, E. M. Mikajlo, and I. Powis, Rev. Sci. Instrum. **76**, 053302 (2005).
[18]W. C. Wiley and I. H. McLaren, Rev. Sci. Instrum. **26**, 1150 (1955).
[19]A. T. J. B. Eppink and D. H. Parker, Rev. Sci. Instrum. **68**, 3477 (1997).
[20]A. Kuthi, P. Gabrielsson, M. R. Behrend, P. T. Vernier, and M. A. Gundersen, IEEE Trans. Plasma Sci. **33**, 1192 (2005).
[21]W. Li, S. D. Chambreau, S. A. Lahankar, and A. G. Suits, Rev. Sci. Instrum. **76**, 063106 (2005).
[22]D. A. Dahl, Int. J. Mass. Spectrom. **200**, 3 (2000); see http://www.simion.com.
[23]C. M Western, PGOPHER, a program for simulating rotational structure, University of Bristol, 2010, see http://pgopher.chm.bris.ac.uk.
[24]A. V. Marenich and J. E. Boggs, J. Chem. Phys. **119**, 10105 (2003).
[25]See supplementary material at http://dx.doi.org/10.1063/1.3685899 for the detailed description of procedures and results of data fittings.
[26]R. J. Bouwens, J. A. Hammerschmidt, M. M. Grzeskowiak, T. A. Stegink, P. M. Yorba, and W. F. Polik, J. Chem. Phys. **104**, 460 (1996).
[27]M. M. Wohar and P. W. Jagodzinski, J. Mol. Spectrosc. **148**, 13 (1991); A. Perrin, J. M. Flaud, A. Predoi-Cross, M. Winnewisser, B. P. Winnewisser, G. Mellau, and M. Lock, J. Mol. Spectrosc. **187**, 61 (1998).
[28]R. Bocquet, J. Demaison, J. Cosléou, A. Friedrich, L. Margulès, S. Macholl, H. Mäder, M. M. Beaky, and G. Winnewisser, J. Mol. Spectrosc. **195**, 345 (1999); K. K. Ellsworth, B. D. Lajiness, J. P. Lajiness, and W. F. Polik, J. Mol. Spectrosc. **252**, 205 (2008).
[29]L. Feng, A. V. Demyanenko, and H. Reisler, J. Chem. Phys. **120**, 6524 (2004).
[30]O. V. Boyarkin, L. Lubich, R. D. F. Settle, D. S. Perry, and T. R. Rizzo, J. Chem. Phys. **107**, 8409 (1997).
[31]A. Geers, J. Kappert, F. Temps, and J. W. Wiebrecht, J. Chem. Phys. **101**, 3618 (1994).
[32]CH_3OH and CD_3OH (Aldrich, 99.5 atom % D) were used without further purification.
[33]The small apparent anisotropy seen in Fig. 1 is caused by nonuniform detection of H fragments created in the dissociation region with different velocity directions. Namely, the light H atoms are fast enough ($\sim 9\ \mu$m/ns) to travel a distance comparable to the laser beam waist radius in few nanoseconds between the radical dissociation and their ionization. Therefore, the detected fraction of vertically ejected fragments is smaller than that of fragments ejected horizontally (and thus remaining within the ionization laser beam). The employed lasers cannot produce pulses shorter than a few nanoseconds, so the average delay can be reduced only by reducing the temporal overlap, when the *end* of the ionization pulse overlaps with the *beginning* of the dissociation pulse. This indeed reduced the apparent anisotropy, but at the expense of significant reduction in the detected signal. SVMI and TOF studies did not show any noticeable dependence on the laser polarization, thus it was concluded that the velocity distributions were isotropic.
[34]To be precise, only the two cases of CH_2OH dissociation can be compared directly, because different masses of the H and D fragments and different moments of inertia of the formaldehyde cofragments should affect the energy partitioning between translations and rotations in the isotopically substituted species. However, these isotopic effects alone cannot explain the almost threefold difference between the rotational temperatures of vibrationless CD_2O and CHDO.
[35]A quantitative measurement of D/H product ratio in CD_2OH dissociation would allow unambiguous estimation of the direct dissociation distribution. However, an accurate measurement is difficult, and the model assumptions do not warrant a more quantitative evaluation. Qualitatively, the D yield was at least an order of magnitude smaller than the H yield, which is consistent with the branching estimated from the model.